JACS
JOURNAL OF THE AMERICAN CHEMICAL SOCIETY
Communication
Cite This: J. Am. Chem. Soc. XXXX, XXX, XXX-XXX
pubs.acs.org/JACS

Ultrahigh Mass Activity for Carbon Dioxide Reduction Enabled by Gold–Iron Core–Shell Nanoparticles

Kun Sun,[†,‡] Tao Cheng,[⊥,‡] Lina Wu,[∥] Yongfeng Hu,[§] Jigang Zhou,[§] Aimee Maclennan,[§] Zhaohua Jiang,[†] Yunzhi Gao,[†] William A. Goddard, III,[*,⊥] and Zhijiang Wang[*,†]

[†]MIIT Key Laboratory of Critical Materials Technology for New Energy Conversion and Storage, School of Chemistry and Chemical Engineering, Harbin Institute of Technology, Harbin 150001, China

[⊥]Materials and Process Simulation Center (MSC) and Joint Center for Artificial Photosynthesis (JCAP), California Institute of Technology, Pasadena, California 91125, United States

[∥]Molecular Imaging Research Center of Harbin Medical University, the Fourth Hospital of Harbin Medical University, Harbin 150001, China

[§]Canadian Light Source Inc., Saskatoon, Saskatchewan S7N 0X4, Canada

Supporting Information

ABSTRACT: Wide application of carbon dioxide (CO_2) electrochemical energy storage requires catalysts with high mass activity. Alloy catalysts can achieve superior performance to single metals while reducing the cost by finely tuning the composition and morphology. We used in silico quantum mechanics rapid screening to identify Au–Fe as a candidate improving CO_2 reduction and then synthesized and tested it experimentally. The synthesized Au–Fe alloy catalyst evolves quickly into a stable Au–Fe core–shell nanoparticle (AuFe-CSNP) after leaching out surface Fe. This AuFe-CSNP exhibits exclusive CO selectivity, long-term stability, nearly a 100-fold increase in mass activity toward CO_2 reduction compared with Au NP, and 0.2 V lower in overpotential. Calculations show that surface defects due to Fe leaching contribute significantly to decrease the overpotential.

Electrochemical reduction of carbon dioxide (CO_2) to value-added products in aqueous solution, especially if driven by solar or wind power sources, provides both a "green" strategy to decrease CO_2 concentration in the atmosphere and an appealing approach to store renewable energy.[1−4] An attractive product for the CO_2 reduction reaction (CO_2RR) is carbon monoxide (CO) because CO has broad applications as a gas precursor for industrial chemical manufacturing. Gold (Au) represents the essential element in reducing CO_2 to CO. As first reported by Hori et al.,[5] Au foils can reduce CO_2 to CO with a Faradaic efficiency (FE) of 87.1% and a partial current density of 4.3 mA/cm^2 at −0.71 V versus the reversible hydrogen electrode (RHE, hereafter all the potential mentioned are referenced to RHE). Such performance can be significantly improved by carefully tuning the sizes,[6−9] shapes,[10−12] and compositions[13−15] of the catalysts. Thus, Liu et al. recently reported an Au needle catalyst with a specific activity reaching 22 mA·cm^{-2} at −0.35 V.[4] However, the high cost of Au remains the primary limiting factor preventing its widespread application in CO_2RR. The mass activities of previously reported Au-based catalysts are all below 3.0 mA/mg at −0.4 V,[16,17] which is far from meeting the requirement of practical applications. Consequently, increasing Au mass activity is highly desired.

We consider here the possibility of alloying Au with a second metal to improve the performance while simultaneously reducing the cost compared to pure Au.[13] Here we used in silico quantum mechanics rapid screening (QM-RS) to search for the best alloy candidates. Using the density functional theory (DFT) Perdew–Burke–Ernzerhof (PBE) flavor of QM, we employed two descriptors in QM-RS: the formation energy of *COOH (* indicates surface site) and the desorption energy of CO. These descriptors were chosen because in our previous studies we established the detail reaction mechanism of CO_2 reduction to CO on copper surface from ab initio molecular dynamics free energy calculations.[18] We found that physisorbed linear CO_2 (l-CO_2) transforms to a chemisorbed CO_2 ($*CO_2^{\delta-}$) that is stabilized by hydrogen bonding to nearby H_2O, then $*CO_2^{\delta-}$ is protonated by a surface H_2O to form *COOH plus surface OH, and then a surface H_2O provides the proton for dehydroxylation of *COOH to form CO plus a surface OH. In this process, the formation energy of *COOH determines the applied potential required to reduce CO_2 to CO, and the desorption energy of CO determines the rate of CO leaving the surface sites to form the product. Thus, we want to decrease both the formation energy of *COOH and the desorption energy of CO to promote CO production.

Due to the thermodynamic stability, we expect that the second metal at the surface will be preferentially leached out during the electrochemical reduction reaction, leaving a pure Au skin covering a binary metallic core.[19,20] Thus, we adopted an (Au surface)-(alloy subsurface) model for the computations (Figure 1A–D). QM-RS was carried out to screen fourth-row and fifth-row transition metals (Sc through Zn and from Y through Cd) forming 1:3 binary alloys with Au. The predictions are shown in Figure 1E. Due to the linear rescaling relationship, a decrease in the formation energy of *COOH is generally at the expense of an increase in desorption energy of CO.[21] Thus,

Received: August 30, 2017
Published: October 9, 2017

DOI: 10.1021/jacs.7b09251
J. Am. Chem. Soc. XXXX, XXX, XXX–XXX

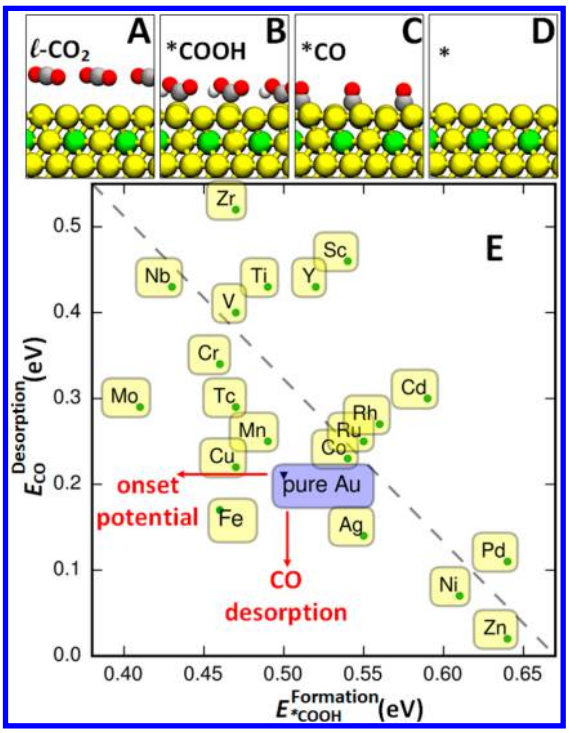

Figure 1. (A–D) Sequence of reaction steps for CO_2RR on gold (Au)–metal (M) binary alloys. The steps are (A) physisorbed CO_2 (*l*-CO_2), (B) *COOH, (C) *CO, (D)* (* indicates surface site). The color codes are Au, yellow; M, green; C, silver; O, red; and H, white. (E) Formation energies of *COOH and desorption energyies of CO for 20 Au–M alloys, where M is a fourth-row transition metal (from Sc to Zn) or fifth-row transition metal (from Y to Cd). For reference, the black triangle (blue shaded) indicates the properties for pure Au.

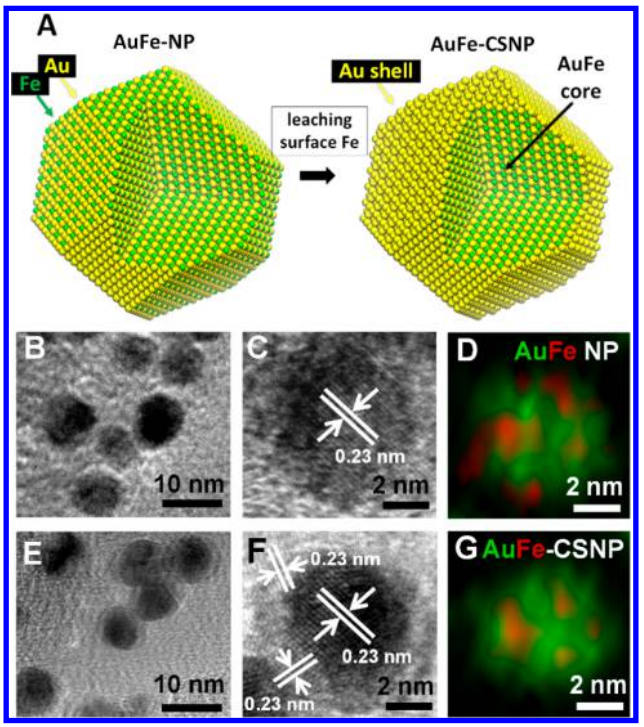

Figure 2. (A) Schematic illustration of the structural evolution of Au–Fe alloy NP to Au–Fe core/Au shell NP after leaching out of surface Fe. Representative TEM and HRTEM images and element map of as-synthesized AuFe-NPs (B–D) and AuFe-CSNP (E–G), respectively. The colors in the element map are green for Au and red for Fe.

we want alloys that break this linear scaling relationship to achieve improved CO_2RR performance. Among the 20 alloys screened, we found that Au–Fe alloy exhibited both a lower formation energy of *COOH (0.46 eV) and a lower desorption energy of CO (0.17 eV), compared with 0.50 and 0.21 eV, respectively for pure Au. Thus, we anticipated that the Au–Fe alloy would improve CO_2RR while reducing the cost.

Hydrogen evolution reaction (HER) is the main side reaction competing with CO_2RR. The presence of surface hydrogen (H*) potentially competes with CO_2 for surface sites. We calculated the adsorption energies of CO_2 and H* (in Table S2), finding that Au–Fe alloy is superior to Au in both promoting CO_2 adsorptions by 0.10 eV and in destabilizing H* adsorption by 0.02 eV.

We then synthesized the Au–Fe alloy NPs using a solvothermal method at 280 °C (more experimental details are in SI). The as-synthesized Au–Fe NPs are about 8.0 nm in diameter (Figure 2B,C) and well-distributed on carbon black support (Figure S1). Such NPs have an *fcc* metal structure as verified by X-ray diffraction patterns (Figure S2) with a lattice spacing of 0.23 nm. As shown in energy-dispersive X-ray (EDX) spectroscopy elemental analysis (Figure 2D), the distribution ranges of Au (green) and Fe (red) almost completely overlap, which indicates that Au and Fe atoms randomly mix in the alloy NPs forming a solid solution structure, consistent with the Au–Fe phase diagram at room temperature.

As expected, significant Fe leaching takes places in the first-hour electrolysis. After that, there are no apparent changes in composition (Figure S6) or morphologies (Figure S7). The sizes of Au–Fe alloy before and after Fe leaching are nearly the same (Figures 2B,C,E,F and S7), which indicates that only a small portion of Fe leached away. EDX mapping of these NPs, as shown in Figures 2G and S3–S4, reveals a core–shell structure that consists of an Au outer layer and Au–Fe alloy inner core. The structure feature is further supported by the X-ray photoelectron spectroscopy (XPS) analysis (Figure S8) showing a much weaker and noisier Fe 3d XPS spectrum of AuFe-CSNP compared to the as-synthesized Au–Fe NP (Figure S5), which indicates that most of the surface Fe have been leached out. A similar result was also observed in Fe K-edge X-ray absorption spectroscopy (XAS) spectra (Figure S9). Therefore, the as-synthesized Au–Fe alloy readily evolves into an Au–Fe core–shell nanoparticle (AuFe-CSNP) under CO_2RR condition.

We carried out extensive CO_2RR of AuFe-CSNPs. Significant CO generation occurs at potentials as low as −0.2 V (Figure 3B). As the applied potential increases to −0.4 V, the partial current density reaches 11.05 mA/cm^2 with an FE of 97.6% (Figure 3A), almost entirely suppressing the HER. Instead, the pure Au NP with similar size (Figure S11) has an insufficient CO_2RR performance with an FE of 30.5% and a partial current density of 0.15 mA/cm^2 at −0.4 V(Figure 3A, 3B and S12), consistent with previous reports (Table S1).[9] Only when the applied voltage reaches −0.7 V does the FE reach 90.8% with a partial current density of 5.72 mA/cm^2 (about half of that AuFe-CSNPs). Taking −0.4 V as a reference potential, the mass activities of AuFe-CSNPs reach 48.2 mA/mg (Figure 3C), almost 100 times higher than that of Au-NPs (0.5 mA/mg) in the same condition.

DOI: 10.1021/jacs.7b09251
J. Am. Chem. Soc. XXXX, XXX, XXX–XXX

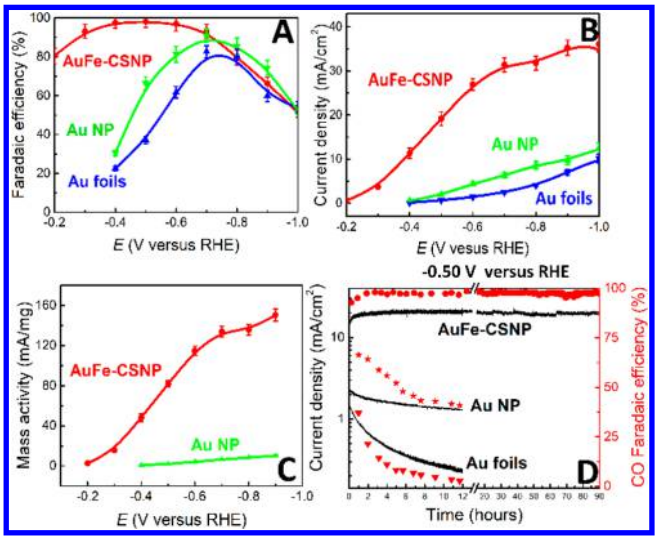

Figure 3. CO_2RR to CO performance of the AuFe-CSNPs, Au-NPs, and Au foils. (A) Faradaic efficiencies (%) at applied potential ranging from $E = -0.2$ V to -1.0 V. (B) Current density (in mA/cm^2). (C) Mass activity (in mA/mg). (D) Durability performance (up to 90 h) at $E = -0.50$ V.

Even after running for 90 h the current density of AuFe CSNPs remains stable at 19.7 mA/cm^2 (Figure 3D). This long-term stability indicates that the core−shell structure is quite stable. DFT calculations show that the diffusion barrier of Au atoms on the pure Au (111) surface is 0.63 eV, which increases slightly to 0.68 eV at the AuFe-CSNP surface (Figure S13). Although the higher diffusion barrier indicates a slower surface diffusion, this 0.05 eV difference in diffusion barriers alone is probably not sufficient to explain the dramatic difference in the stability of the FE. Instead, we suspect that making the AuFe NP and then leaching the Fe from the surface builds in a more stable dimpled Au surface structure than merely forming the Au NP or forming an Au film, because the surface skin may prevent the diffusion from interior. Such long-term stability is a substantial improvement over Au NPs and Au foil. Au NPs and Au foil deactivate quickly within 12 h by losing about 55% (from 2.8 mA/cm^2 dropping to 1.26 mA/cm^2) and 87% (from 1.69 mA/cm^2 dropping to 0.22 mA/cm^2) in the current density, respectively.

AuFe-CSNPs reduces the onset potential by 0.2 V (−0.2 V vs −0.4 V), about 0.14 V lower than we predicted from the DFT calculations. Thus, the subsurface alloy effect alone cannot fully explain the superior performance. Instead, we suspected that the additional lowering in overpotential might arise from surface defects due to Fe leaching. The presence of surface defects is supported by the experiment Au L_3 EXAFS (Figure S10). In the Fourier transform, the peaks corresponding to Au−Au bonding (from 2.0 to 3.2 Å) shift to lower R and reduce in intensity. Such variations in EXAFS may attribute to either sharply reduced particle size or the existence of surface defects.[22] Because AuFe-CSNPs have a core size quite similar to pristine Au−Fe NP, the only reasonable explanation is that numerous vacancies lie on the Au surface layer of AuFe-CSNPs. Therefore, leaching surface Fe leads to the formation of a core−shell structure with jagged surface, which possess highly active sites as we demonstrated previously that jagged Pt nanowires exhibit superior mass activity performance in reducing oxygen to water.[23] To estimate the effect of such defects on CO_2RR, we carried out a PBE DFT calculations on an extreme case by removing one surface Au atom to create a Schottky defect (as shown in Figure 4A,B). We estimated that such surface defect

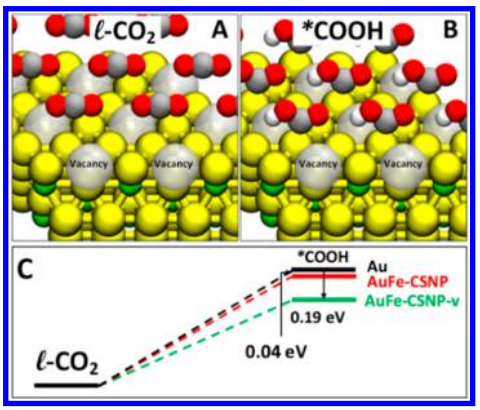

Figure 4. (A) l-CO_2 and (B) *COOH are on the surface with vacancies. (C) Diagram of formation energies of *COOH (the potential determining step for CO_2RR) in pure Au (in black), AuFe-CSNP (in red), and AuFe-CSNP with vacancies (AuFe-CSNP-v, in green).

could decrease the formation energy of *COOH by 0.19 eV (Figure 4C), which is roughly consistent with the experimentally observed 0.2 V decrease in onset potential. We also demonstrated the effect of Schotttky defect on pure Au and Au−Cu alloy and predicted a 0.29 and 0.24 eV decrease in *COOH formation. Thus, the existence of a surface defect is beneficial to CO_2RR, while stabilizing these surface defects is equally important. Au−Fe CSNPs exhibit both of these characters.

In summary, we used rapid computational screening to identify AuFe as the best alloy among 20 metals for CO_2RR at low overpotential. Such AuFe alloys exhibit outstanding CO_2RR performance after evolving into a core−shell structure due to leaching of surface Fe. At −0.40 V (RHE), the core−shell structure reduces CO_2 exclusively to CO, with HER almost entirely suppressed. The mass activity of this AuFe-CSNP catalyst reaches 48.2 mA/mg, ∼100 times better than previously reported Au-NP catalysts. Moreover, this AuFe-CSNP exhibits long-term catalysis efficiency, with the performance remaining almost constant in the 90 h duration test. Our QM calculations suggest that this excellent performance toward CO_2RR arises from subsurface Fe combined with surface defects due to surface Fe leaching.

■ ASSOCIATED CONTENT

Supporting Information

The Supporting Information is available free of charge on the ACS Publications website at DOI: 10.1021/jacs.7b09251.

Materials and Methods, Figures S1−S13, and Tables S1−S2. (PDF)

■ AUTHOR INFORMATION

Corresponding Authors

*wangzhijiang@hit.edu.cn

*wag@wag.caltech.edu

ORCID

Tao Cheng: 0000-0003-4830-177X

Jigang Zhou: 0000-0001-6644-2862

William A. Goddard III: 0000-0003-0097-5716

DOI: 10.1021/jacs.7b09251
J. Am. Chem. Soc. XXXX, XXX, XXX−XXX

Zhijiang Wang: 0000-0001-9314-7922

Author Contributions

‡These authors contributed equally.

Notes

The authors declare no competing financial interest.

■ ACKNOWLEDGMENTS

T.C. and W.A.G. were supported by the Joint Center for Artificial Photosynthesis, a DOE Energy Innovation Hub, supported through the Office of Science of the U.S. Department of Energy under award no. DE-SC0004993. Z.W. acknowledges Mr. David Muir for his kind help on the EXAFS measurement and financial support from the National Natural Science Foundation of China (no. 51572062) and the Natural Science Foundation of Heilongjiang Province (no. B2015002). L.W. appreciates the financial support of National Natural Science Foundation of China (no. 81771903), Heilongjiang Province Foundation for Returness (no. LC2016034), and Wuliande Foundation of Harbin Medical University (grant no. WLD-QN1404). C.L.S. is supported by the NSERC, NRC, CIHR of Canada, and the University of Saskatchewan. The QM calculations used the resources of the Extreme Science and Engineering Discovery Environment (XSEDE) which is supported by National Science Foundation grant no. ACI-1053575.

■ REFERENCES

(1) Olah, G. A.; Prakash, G. K. S.; Goeppert, A. *J. Am. Chem. Soc.* **2011**, *133* (33), 12881−12898.
(2) Montoya, J. H.; Seitz, L. C.; Chakthranont, P.; Vojvodic, A.; Jaramillo, T. F.; Norskov, J. K. *Nat. Mater.* **2017**, *16* (1), 70−81.
(3) Rosen, B. A.; Salehi-Khojin, A.; Thorson, M. R.; Zhu, W.; Whipple, D. T.; Kenis, P. J. A.; Masel, R. I. *Science* **2011**, *334* (6056), 643−644.
(4) Liu, M.; Pang, Y.; Zhang, B.; De Luna, P.; Voznyy, O.; Xu, J.; Zheng, X.; Dinh, C. T.; Fan, F.; Cao, C.; de Arquer, F. P. G.; Safaei, T. S.; Mepham, A.; Klinkova, A.; Kumacheva, E.; Filleter, T.; Sinton, D.; Kelley, S. O.; Sargent, E. H. *Nature* **2016**, *537* (7620), 382−386.
(5) Hori, Y.; Murata, A.; Kikuchi, K.; Suzuki, S. *J. Chem. Soc., Chem. Commun.* **1987**, *10* (10), 728−729.
(6) Hall, A. S.; Yoon, Y.; Wuttig, A.; Surendranath, Y. *J. Am. Chem. Soc.* **2015**, *137* (47), 14834−14837.
(7) Mistry, H.; Reske, R.; Zeng, Z.; Zhao, Z.-J.; Greeley, J.; Strasser, P.; Cuenya, B. R. *J. Am. Chem. Soc.* **2014**, *136* (47), 16473−16476.
(8) Chen, Y.; Li, C. W.; Kanan, M. W. *J. Am. Chem. Soc.* **2012**, *134* (49), 19969−19972.
(9) Zhu, W.; Michalsky, R.; Metin, Ö.; Lv, H.; Guo, S.; Wright, C. J.; Sun, X.; Peterson, A. A.; Sun, S. *J. Am. Chem. Soc.* **2013**, *135* (45), 16833−16836.
(10) Zhu, W. L.; Zhang, Y. J.; Zhang, H. Y.; Lv, H. F.; Li, Q.; Michalsky, R.; Peterson, A. A.; Sun, S. H. *J. Am. Chem. Soc.* **2014**, *136* (46), 16132−16135.
(11) Saberi Safaei, T.; Mepham, A.; Zheng, X.; Pang, Y.; Dinh, C.-T.; Liu, M.; Sinton, D.; Kelley, S. O.; Sargent, E. H. *Nano Lett.* **2016**, *16* (11), 7224−7228.
(12) Back, S.; Yeom, M. S.; Jung, Y. *ACS Catal.* **2015**, *5* (9), 5089−5096.
(13) Kim, D.; Resasco, J.; Yu, Y.; Asiri, A. M.; Yang, P. *Nat. Commun.* **2014**, *5*, 4948.
(14) Ma, S.; Sadakiyo, M.; Heima, M.; Luo, R.; Haasch, R. T.; Gold, J. I.; Yamauchi, M.; Kenis, P. J. A. *J. Am. Chem. Soc.* **2017**, *139* (1), 47−50.
(15) Sun, K.; Wu, L.; Qin, W.; Zhou, J.; Hu, Y.; Jiang, Z.; Shen, B.; Wang, Z. *J. Mater. Chem. A* **2016**, *4* (32), 12616−12623.
(16) Kim, C.; Jeon, H. S.; Eom, T.; Jee, M. S.; Kim, H.; Friend, C. M.; Min, B. K.; Hwang, Y. J. *J. Am. Chem. Soc.* **2015**, *137* (43), 13844−13850.
(17) Lu, Q.; Rosen, J.; Zhou, Y.; Hutchings, G. S.; Kimmel, Y. C.; Chen, J. G.; Jiao, F. *Nat. Commun.* **2014**, *5*, 3242.
(18) Cheng, T.; Xiao, H.; Goddard, W. A. *J. Am. Chem. Soc.* **2016**, *138* (42), 13802−13805.
(19) Ghosh Chaudhuri, R.; Paria, S. *Chem. Rev.* **2012**, *112* (4), 2373−2433.
(20) Ban, Z.; Barnakov, Y. A.; Li, F.; Golub, V. O.; O'Connor, C. J. *J. Mater. Chem.* **2005**, *15* (43), 4660−4662.
(21) Hansen, H. A.; Shi, C.; Lausche, A. C.; Peterson, A. A.; Norskov, J. K. *Phys. Chem. Chem. Phys.* **2016**, *18* (13), 9194−9201.
(22) Zhang, P.; Zhou, X.; Tang, Y.; Sham, T. K. *Langmuir* **2005**, *21* (18), 8502−8508.
(23) Li, M.; Zhao, Z.; Cheng, T.; Fortunelli, A.; Chen, C.-Y.; Yu, R.; Zhang, Q.; Gu, L.; Merinov, B. V.; Lin, Z.; Zhu, E.; Yu, T.; Jia, Q.; Guo, J.; Zhang, L.; Goddard, W. A.; Huang, Y.; Duan, X. *Science* **2016**, *354* (6318), 1414−1419.

DOI: 10.1021/jacs.7b09251
J. Am. Chem. Soc. XXXX, XXX, XXX−XXX